Eur. Phys. J. A **22**, 471–480 (2004)
DOI 10.1140/epja/i2004-10051-7

THE EUROPEAN PHYSICAL JOURNAL A

Fast helium production in interactions of 3.7 A GeV ^{24}Mg with emulsion nuclei

M.A. Jilany[a]

Physics Department, Faculty of Science (Sohag), South Valley University, Sohag, Egypt

Received: 6 April 2004 / Revised version: 13 July 2004 /
Published online: 19 November 2004 –
Communicated by A. Molinari

Abstract. We have studied the properties of the relativistic helium fragments emitted from the projectile in the interactions of ^{24}Mg ions accelerated at an energy of 3.7 A GeV with emulsion nuclei. The total, partial nuclear cross-sections and production rates of helium fragmentation channels in relativistic nucleus-nucleus collisions and their dependence on the mass and energy of the incident projectile nucleus are investigated. The yields of multiple helium projectile fragments disrupted from the interactions of ^{24}Mg projectile nuclei with hydrogen H, light CNO and heavy AgBr groups of target emulsion nuclei are discussed and they indicate that the breakup mechanism of the projectile seems to be independent of the target mass. Limiting fragmentation behavior of fast-moving helium fragments is observed in both the projectile and target nuclei. The multiplicity distributions of helium projectile fragments emitted in the interactions of ^{24}Mg projectile nuclei with the different target nuclei of the emulsion are well described by the KNO scaling presentation. The mean multiplicities of the different charged secondary particles, normally defined shower, grey and black ($\langle n_{\rm s}\rangle$, $\langle n_{\rm g}\rangle$ and $\langle n_{\rm b}\rangle$) emitted in the interactions of 3.7 A GeV ^{24}Mg with the different groups of emulsion nuclei at different ranges of projectile fragments are decreasing when the number of He fragments stripped from projectile increases. These values of $\langle n_{\rm i}\rangle$ (i = s, g, b and h particles) in the events where the emission of fast helium fragments were accompanied by heavy fragments having $Z \geqslant 3$ seem to be constant as the He multiplicity increases, and exhibit a behavior independent of the He multiplicity.

PACS. 29.40.Rg Nuclear emulsions – 25.75.-q Relativistic heavy-ion collisions – 25.70.Mn Projectile and target fragmentation – 25.70.Pq Multifragment emission and correlations

1 Introduction

The study of relativistic nucleus-nucleus (AA) collisions, which has been carried out quite actively in recent years, can be the source of interesting information on the deep properties of matter. In collisions of nuclei, the compression of nuclear matter results in the production of particles, and the system expands and may disassemble into multifragments. Multifragmentation has been considered to be one of the most important aspects of heavy-ion collisions since it has been speculated that the decay of a highly excited nuclear system might carry information about the equation of state [1–5]. Multifragmentation was predicted to be the dominant decay mode at excitation energies near the binding energy of nuclei of about 8 MeV per nucleon and at densities below the saturation density of nuclear matter [6,7].

The excited piece of nuclear matter decays predominantly by the emission of nucleons, deuterons, tritons, helium nuclei, intermediate mass fragments and heavy charged fragments [8], depending on the target-projectile combination and on the beam energy. Helium nuclei, probably mostly alpha particles, may have several sources in relativistic reactions: they can derive from some direct knock-out reactions due to the short-range correlations (alpha-clustering) in the incoming projectile of hard-scattered nucleons which may undergo coalescence and, predominantly, excited remnants will break up with Q-values that are much lower for alpha decay than for the other particle emission channels. To understand the dynamics involving the formation of helium, intermediate and heavy fragments in the final state, numerous experiments have been performed in nucleus-nucleus interactions at low, intermediate and high energies [2,9–13]. The decay properties of nuclei produced in these interactions indicate that a high degree of equilibrium has been reached. This is a prerequisite for the study of the thermodynamic behavior of highly excited nuclear matter and makes these reactions rather attractive for this purpose [14].

[a] e-mail: majilany@hotmail.com

On the other hand, the fragment distribution can be described statistically by considering all the possible partition of A nucleons into smaller clusters. This study gives a tool for the description of nuclear multifragmentation distributions, nuclear liquid-gas phase transition, critical exponent, intermittency and chaotic behavior of nuclear multifragmentation [15]. To explain the experimental results on the still debated subject of nuclear multifragmentation, several alternative theoretical approaches [6,7] have been put forward, in which the formation and decay of intermediate mass fragments are assumed to take place through statistical or dynamical processes [16–18]. Thus, more experimental information is clearly required in order to disentangle various existing models on this interesting topic of multifragmentation [2].

The study of global and local multiplicities of projectile and target fragments produced in collisions between heavy ions is important for several reasons. To a large extent these variables are determined by the geometry of the interactions. Understanding the effects of the geometry is crucial in order to distinguish subtle phenomena, such as a possible creation of quark-gluon plasma, from more elementary processes. These variables are also useful tools for the understanding of the reaction mechanisms. Systematic studies of the variation with mass, energy, and impact parameter can be used for predictions of heavier systems and to elucidate the importance of rescattering [19]. It is obvious that large systems can fragment in a larger number of fragments than the smaller one and the same is true for corresponding fluctuations. So for a more realistic comparison of the fragmentation of different systems the corresponding multiplicity distributions must be scaled. Multiplicity distributions at different beam energies are conveniently compared using the Koba, Nielsen and Olesen scaling hypothesis [20]. These authors put forward the hypothesis that at relativistic and ultra relativistic energies the probability distributions P_n of producing n particles in a certain collision process should exhibit the scaling relation

$$P_n = \frac{1}{\langle n \rangle} \Psi \left(\frac{n}{\langle n \rangle} \right) \tag{1}$$

with $\langle n \rangle$ being the average multiplicity of secondaries. This so-called KNO scaling hypothesis asserts that if one rescale P_n measured at different energies via stretching (shrinking) the vertical (horizontal) axes by $\langle n \rangle$, these rescaled curves will coincide with each other, that is, the multiplicity distributions become simple rescale copies of the universal function $\Psi(Z)$, which will depend only on the scaled multiplicity $Z = n/\langle n \rangle$. In the picturesque terminology of Stanley [21] the rescaled data points P_n measured at different energies collapse onto the unique scaling curve $\Psi(Z)$.

In the present paper we pay particular attention to the properties of fast-moving helium fragments that stripped in interactions of the ^{24}Mg projectile with the target nuclei in nuclear emulsion (Em) at 3.7 A GeV. The multiplicity scaling of these helium projectile fragments is also investigated in the framework of the KNO scaling. This study is complementary to a very recent one [3], which deals with the production and characteristics of nuclear fragmentation channels in ^{24}Mg projectile on emulsion targets.

2 Scanning procedures

Standard stacks of NIKFI BR-2 nuclear emulsion pellicles of $20 \times 10 \times 0.06$ cm^3 in volume, with a sensitivity of 30 grains per 100 μm for a singly charged minimum-ionizing particle, have been exposed horizontally to the Dubna Synchrophasotron ^{24}Mg beam at an energy of 3.7 A GeV. The density of the beam was about 10^4 nuclei/cm^2.

Interactions were found by along-the-track double scanning, which is the optimal method for obtaining a minimum-bias sample. Each projectile was followed up to a distance of 6 to 7 cm from the incident edge of the pellicle and was carefully observed until the ^{24}Mg primary either interacted or escaped from the pellicle. One thousand and twenty-five minimum bias inelastic events giving a mean free path of 9.61 ± 0.30 cm have been located. For this investigation, a total of 515 peripheral events having at least one helium fragment originating from the magnesium projectile in a narrow forward cone have been selected. For each event the multiplicity of shower particles ($n_{\rm s}$) and of target associated particles ($n_{\rm h}$) was determined. The shower particles are singly charged relativistic particles with a velocity $\beta \geqslant 0.7$ and ionization less than 1.4 times the plateau ionization for the singly charged minimum-ionizing particles, outside the projectile fragmentation cone. Most of these particles are pions with energies above 70 MeV contaminated with small proportions of fast protons with energies above 400 MeV. The heavily ionizing particles ($n_{\rm h}$) with a velocity $\beta < 0.7$ are known as black ($n_{\rm b}$) and grey ($n_{\rm g}$) particles. $n_{\rm b}$-particles are charged particles having a velocity $\beta < 0.3$ with a residual range $L \leqslant 3$ mm in emulsion. Generally, $n_{\rm b}$ particles are protons of kinetic energies $E \leqslant 26$ MeV and are the fragments evaporated from the target emulsion. $n_{\rm g}$-particles have a velocity $0.3 < \beta < 0.7$ with a residual range of $L > 3$ mm in emulsion. These particles are predominantly recoil target protons in the kinetic energy range $26 < E < 400$ MeV and occasionally kaons and π-mesons. The multiplicity of heavy tracks ($n_{\rm h}$) is generally defined as $n_{\rm h} = n_{\rm b} + n_{\rm g}$ [2].

At relativistic energies, multiple charged fragments with charge $Z \geqslant 2$ emitted from the breakup of the projectile essentially travel with the same speed of the beam. These energetic projectile fragments (PFs) are recorded in emulsion with 100% detection efficiency and this intrinsic feature of emulsion makes it a unique detector among all the particle detectors currently in use [2].

The distinction between the projectile and the target spectator fragments is easy to make. The projectile-like fragments corresponding to the spectator part are distributed in a forward narrow cone, while the emitted particles and rescattered protons have a much broader distribution. The fragments emitted from the target are observed as highly ionizing particles, isotropically distributed. They can be black particles which are essentially fragments evaporated from the target, with a range $L \leqslant 3$ mm, or

gray particles, that is knock-out protons or slow mesons with a range $L > 3$ mm [8].

A total of 880 He-projectile tracks were selected in 515 peripheral inelastic events. In each event, we recorded the multiplicity of fast singly charged particles $n_{\rm p}$ and the multiplicity fragments emitted from projectile like helium n_α, as well as the heavier products $n_{\rm f}$ with charge $Z \geqslant 3$, that are emitted within the fragmentation cone defined by a critical angle, which is at 3.7 A GeV $\theta_{\rm c} \approx 3^\circ$ [22]. The charges of the projectile fragments $Z \geqslant 2$ were determined by the delta-rays-counting method along the beam track and the tracks of each of the outgoing fragments [22].

Since the nuclear emulsion is a composite target, the incident ^{24}Mg projectile will interact with either one of the following components: the free hydrogen (H, $A_{\rm t} = 1$), the light (CNO, $A_{\rm t} = 14$) and the heavy (AgBr, $A_{\rm t} = 94$) nuclei. An important parameter, which is easy to obtain experimentally, and greatly helps in this respect, is the number of heavily ionizing particles $n_{\rm h}$ emitted from the target nucleus. Depending upon the target break-up, the authors of refs. [11,23,24] have proposed the separation technique of these interactions, which will be used in the present work according to the following criteria:

i) Events with $n_{\rm h} = 0$, 1: include all ^{24}Mg-H interactions but also some of the peripheral interactions of ^{24}Mg-CNO and the very peripheral interactions of ^{24}Mg-AgBr.
ii) Events with $2 \leqslant n_{\rm h} \leqslant 7$: they contain mainly the remaining interactions of ^{24}Mg-CNO not included in i), together with some admixture of peripheral ^{24}Mg-AgBr interactions.
iii) All events with $n_{\rm h} \geqslant 8$ are only the remaining interactions of ^{24}Mg-AgBr.

This separation of ^{24}Mg-Em interactions allowed us to make simultaneous analysis of the fragmentation processes of both projectile and target nuclei as well as to study the production processes as a function of the target mass, taking full advantage of the nuclear emulsion technique. Using the above criteria, the total 1025 interactions of ^{24}Mg projectile with emulsion target nuclei are classified into 211 events with $n_{\rm h} = 0$–1 mainly due to ^{24}Mg-H, 363 events with $n_{\rm h} = 2$–7 mainly due to ^{24}Mg-CNO and 451 events with $n_{\rm h} \geqslant 8$ due to ^{24}Mg-AgBr interactions.

3 Results

The measured value of the nuclear projectile-target cross-section $\sigma_{\rm nuc}^{A_{\rm p}A_{\rm t}}$ in the interactions of primary ^{24}Mg beam with emulsion nuclei at 3.7 A GeV has been compared with those obtained in a wide range of interactions of different projectiles (from ^{4}He up to ^{208}Pb) with emulsion target nuclei at different energies. The dependence of the nuclear cross-section of the projectile-target system $\sigma_{\rm nuc}^{A_{\rm p}A_{\rm t}}$ on the masses of the projectile ($A_{\rm p}$) and target ($A_{\rm t}$) can be investigated according to the Bradt and Peters [25] formula, through which at high incident energies the nuclear inelastic cross-section for nucleus-nucleus (AA) interactions can be parameterized by a simple geometrical

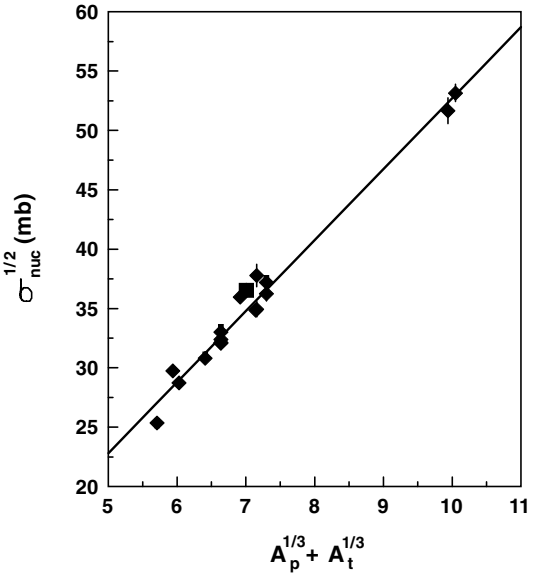

Fig. 1. Dependence of the square root of the experimental nuclear cross-section on $A_{\rm p}^{1/3} + A_{\rm t}^{1/3}$ for several projectiles on the target emulsion nuclei: 3.7 A GeV ^{24}Mg (solid square - present work), 3.7 A GeV ^{4}He [26], 3.7 A GeV ^{6}Li [27], 3.0 A GeV ^{7}Li [28], 3.7 A GeV ^{12}C [29], (3.7 A GeV [28], 14.6, 60 and 200 A GeV [30]) ^{16}O, 3.3 A GeV ^{22}Ne [31], (3.7 A GeV [22], 3.7 A GeV [32] and 14.6 A GeV [33]) ^{28}Si, (3.7 A GeV [34] and 200 A GeV [35]) ^{32}S, 10.6 A GeV ^{197}Au [12] and 160 A GeV ^{208}Pb [2]. The straight line represents the best fit to the relation (2) (see text).

formula

$$\sigma_{\rm nuc}^{A_{\rm p}A_{\rm t}} = \pi r_0^2 \left(A_{\rm p}^{1/3} + A_{\rm t}^{1/3} - b\right)^2 , \qquad (2a)$$

where r_0 is the interaction-radius and b is a parameter connected to the transparency of the nuclei or overlap parameter. b can be obtained by fitting the previous formula with the experimental data of different projectiles at various energies. Figure 1 illustrates the square root of the experimental nuclear cross-sections $\sigma_{\rm nuc}^{A_{\rm p}A_{\rm t}}$ as a function of $(A_{\rm p}^{1/3} + A_{\rm t}^{1/3})$ for the interactions concerning the present work (^{24}Mg beam), together with data obtained with different projectiles on emulsion nuclei in the energy range from 3 A GeV up to 200 A GeV: ^{4}He from ref. [26], ^{6}Li from [27], ^{7}Li from [28], ^{12}C from [29], ^{16}O from [28,30], ^{22}Ne from [31], ^{28}Si from [22, 32, 33], ^{32}S from [34, 35], ^{197}Au from [12] and ^{208}Pb from [2]. The nuclear cross-sections $\sigma_{\rm nuc}^{A_{\rm p}A_{\rm t}}$ are seen to depend substantially only on the masses of colliding nuclei, with a linear behavior, while they result almost energy independent. A linear fit can be used to reproduce the data, with the fitting parameters:

$$r_0 = 1.38 \pm 0.02\,\text{fm} \quad \text{and} \quad b = 1.17 \pm 0.07\,. \qquad (2b)$$

Table 1 illustrates the partial and the total nuclear cross-sections of multiple helium ($\sigma_{n\rm He}$) events of ^{24}Mg interactions with H, CNO, Em and AgBr groups of target nuclei at 3.7 A GeV in comparison with the corresponding

Table 1. The partial production cross-sections of fast-helium-fragments channels emitted in the interactions of ^{24}Mg, ^{28}Si, ^{32}S, ^{197}Au and ^{208}Pb projectiles with target emulsion nuclei at different energies.

Projectile + Target	^{24}Mg + H	^{24}Mg + CNO	^{24}Mg + Em	^{24}Mg + AgBr	^{28}Si + Em	^{28}Si + Em	^{32}S + Em	^{197}Au + Em	^{208}Pb + Em
Energy (A GeV)	3.7	3.7	3.7	3.7	3.7	14.6	200	10.6	160
$\sigma_{1\alpha}$ (mb)	193 ± 19	382 ± 28	367 ± 25	557 ± 33	341 ± 15	325 ± 21	345 ± 19	267 ± 24	281 ± 29
$\sigma_{2\alpha}$ (mb)	111 ± 13	209 ± 21	194 ± 17	313 ± 27	199 ± 11	171 ± 16	171 ± 17	250 ± 22	301 ± 30
$\sigma_{3\alpha}$ (mb)	63 ± 11	60 ± 11	63 ± 9	59 ± 10	98 ± 8	70 ± 10	81 ± 9	310 ± 30	273 ± 28
$\sigma_{4\alpha}$ (mb)	37 ± 9	35 ± 8	35 ± 7	30 ± 7	30 ± 4	21 ± 5	28 ± 5	321 ± 36	320 ± 31
$\sigma_{5\alpha}$ (mb)	13 ± 5	13 ± 4	12 ± 4	10 ± 3	9 ± 2	14 ± 5	8 ± 3	258 ± 23	268 ± 28
$\sigma_{6\alpha}$ (mb)					4 ± 2	1 ± 1	4 ± 2	194 ± 20	183 ± 23
$\sigma_{7\alpha}$ (mb)								176 ± 18	180 ± 23
$\sigma_{8\alpha}$ (mb)								136 ± 15	107 ± 18
$\sigma_{9\alpha}$ (mb)								101 ± 14	82 ± 15
$\sigma_{10\alpha}$ (mb)								71 ± 13	41 ± 11
$\sigma_{11\alpha}$ (mb)								33 ± 8	41 ± 11
$\sigma_{12\alpha}$ (mb)								8 ± 4	11 ± 5
$\sigma_{13\alpha}$ (mb)								10 ± 4	6 ± 4
$\sigma_{14\alpha}$ (mb)								4 ± 3	–
$\sigma_{15\alpha}$ (mb)								4 ± 3	3 ± 2
$\sigma_{16\alpha}$ (mb)								4 ± 3	–
σ_{Tot} (mb)	417 ± 21	699 ± 33	671 ± 28	969 ± 42	680 ± 20	605 ± 29	636 ± 25	2147 ± 69	2097 ± 58
Reference	Present work	Present work	Present work	Present work	[32]	[36]	[37]	[8]	[2]

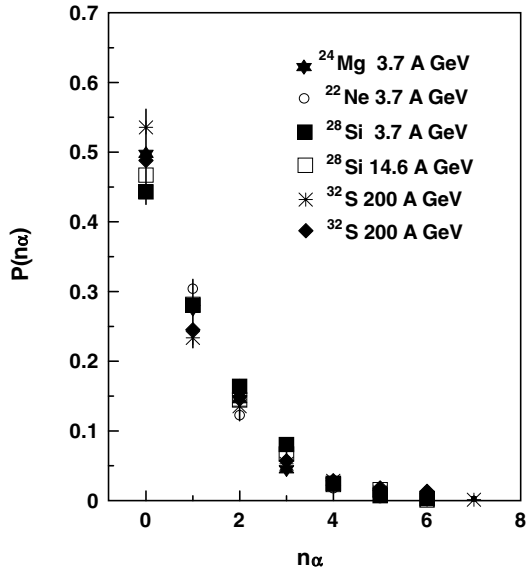

Fig. 2. The normalized multiplicity distributions of fast-moving helium fragments emitted in the nuclear interactions of different projectiles with the target emulsion nuclei at various incident energies (see text for details).

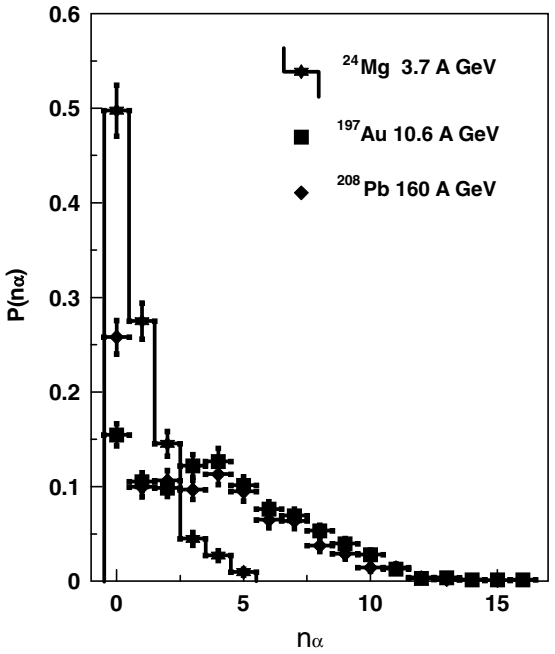

Fig. 3. Dependence of the multiplicity distributions of relativistic helium fragments on the projectile mass for 3.7 A GeV ^{24}Mg, 10.6 A GeV ^{197}Au [8] and 160 A GeV ^{208}Pb [2] with the emulsion nuclei.

values of other systems at different energies. The total and partial nuclear cross-sections of helium emission channels for ^{24}Mg, ^{28}Si and ^{32}S primary beams incident on emulsion nuclei result to be, within experimental errors, the same at different energies. Similar results are obtained when comparing the 10.6 A GeV ^{197}Au and 160 A GeV ^{208}Pb reactions. For $n_\alpha = 1$ and 2, the cross-sections depend strongly on the mass of the target. The helium production cross-sections result to be energy independent, but increasing with the increasing of the mass of both projectile and target.

Table 2. The average multiplicity $\langle n_\alpha \rangle$, the dispersion D, the ratio $\langle n_\alpha \rangle / D$, the C_q moments and the second Muller moment F_2 for helium fragments emitted from projectile in different nucleus-nucleus collisions at various energies.

Reaction	Energy (A GeV)	$\langle n_\alpha \rangle$	D	$\frac{\langle n_\alpha \rangle}{D}$	C_2	C_3	C_4	C_5	F_2	Ref.
^{12}C-Em	3.7	1.49 0.13	0.67± 0.06	2.22± 0.19	1.20± 0.10	1.71± 0.15	2.72± 0.23	4.68± 0.40	1.04± 0.09	[40]
^{16}O-Em	60	1.60± 0.10	0.90± 0.10	1.80± 0.20	1.20± 0.10	1.80± 0.10	2.90± 0.20	4.90± 0.30	1.00± 0.10	[37]
^{22}Ne-Em	3.7	1.60± 0.03	0.86± 0.02	1.85± 0.04	1.29± 0.03	2.09± 0.05	3.99± 0.09	8.47± 0.18	0.86± 0.02	[40]
^{24}Mg-H	3.7	1.95± 0.11	1.25± 0.08	1.56± 0.12	1.33± 0.08	2.18± 0.12	4.08± 0.22	8.33± 0.47	0.70± 0.04	Present work
^{24}Mg-CNO	3.7	1.57± 0.05	0.67± 0.03	2.36± 0.15	1.27± 0.04	2.04± 0.07	3.97± 0.13	8.95± 0.29	0.90± 0.03	Present work
^{24}Mg-Em	3.7	1.71± 0.04	0.94± 0.03	1.82± 0.06	1.32± 0.03	2.24± 0.06	4.50± 0.11	10.11± 0.25	0.77± 0.02	present work
^{24}Mg-AgBr	3.7	1.72± 0.07	0.96± 0.05	1.79± 0.09	1.33± 0.05	2.26± 0.09	4.58± 0.18	10.35± 0.41	0.74± 0.03	Present work
^{28}Si-Em	3.7	1.79± 0.04	0.98± 0.02	1.83± 0.07	1.31± 0.03	2.15± 0.05	4.20± 0.09	9.36± 0.19	0.80± 0.02	[32]
^{28}Si-Em	14.6	1.78± 0.05	1.09± 0.03	1.63± 0.08	1.34± 0.04	2.31± 0.07	4.71± 0.14	10.74± 0.32	0.70± 0.02	[32]
^{28}Si-Em	14.6	1.70± 0.10	1.00± 0.10	1.80± 0.10	1.30± 0.10	2.30± 0.10	4.60± 0.20	10.60± 0.50	0.80± 0.10	[36]
^{32}S-Em	200	1.83± 0.06	1.18± 0.05	1.55± 0.07	1.35± 0.05	2.35± 0.08	4.95± 0.17	11.90± 0.42	0.66± 0.03	[32]
^{197}Au-Em	10.6	4.72± 0.24	7.83± 0.17	0.60± 0.05	1.35± 0.07	2.21± 0.11	4.13± 0.21	8.58± 0.44	3.08± 0.16	[8]
^{208}Pb-Em	160	4.47± 0.26	7.13± 0.18	0.63± 0.06	1.37± 0.08	2.22± 0.13	4.13± 0.24	8.44± 0.49	2.92± 0.17	[2]

Figure 2 represents the comparison of the normalized multiplicity distributions of helium fragments obtained in the present work with ^{24}Mg projectile with respect to those obtained for ^{22}Ne, ^{28}Si, ^{32}S projectiles with emulsions at different energies. Again, the production rates of helium fragments are approximately the same and independent of the beam energy; they show that the limiting fragmentation hypothesis holds. The probability of having one helium fragment emitted from the projectile is around 50% of the total events, in which helium products are present and it is the dominant process in all the considered reactions, showing a picture independent of energy. The probability of emission of two and three helium fragments per event is about 30% and 10%, respectively, of the total helium events.

The multiplicity distributions of helium fragments is shown in fig. 3 for the present work (3.7 A GeV ^{24}Mg) and for those data obtained from the 10.6 A GeV ^{197}Au and 160 A GeV ^{208}Pb. In ^{197}Au-Em and ^{208}Pb-Em interactions one observes events with large values of n_α up to $n_\alpha = 16$, which are absent in the ^{24}Mg-Em interactions ($n_\alpha = 5$). In general, the multiplicity distributions of helium projectile fragments become much broader (larger dispersion) with the increase of the projectile mass. This broadening is physically expected since the number of participant helium clusters becomes larger for larger projectile as we can clearly see when comparing mean multiplicities and dispersions (see table 2), indicating that the disruption mechanism of the projectile into clusters of He fragments may be dependent on the projectile energy or size or both.

The different multiplicity distributions of fragments obtained from the different interactions of ^{24}Mg nuclei with hydrogen H, light CNO and heavy AgBr groups of emulsion nuclei are illustrated in fig. 4. Within experimental errors, no significant difference is evident and the most probable events were those where one or two alphas were produced. Nevertheless small differences may be underlined: the probability of emission is more pronounced for $n_\alpha = 1$ and 2, in case of the interactions of ^{24}Mg with heavy target nuclei (AgBr; the most violent high-temperature processes) than in the case of interactions with light nuclei (H, CNO; the gentle low-temperature processes). The difference in the yields of $n_\alpha = 3$ and $n_\alpha = 4$ may depend on the target within the errors bars: it can be seen that, larger $P(n_\alpha)$ are related to the H target

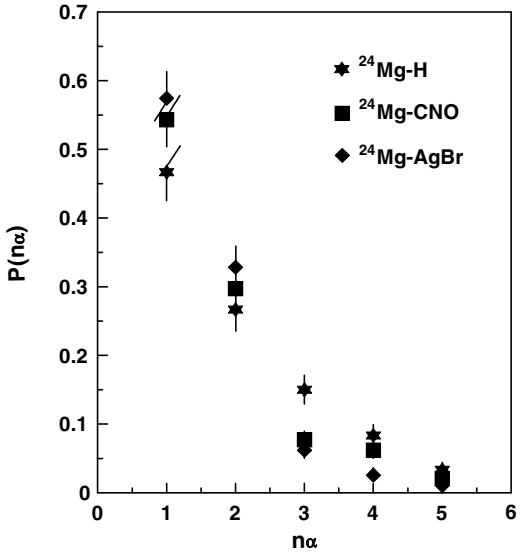

Fig. 4. Distributions of multiple helium projectile fragments emitted in the interactions of ^{24}Mg nuclei with hydrogen H, light CNO and heavy AgBr groups of emulsion nuclei at 3.7 A GeV.

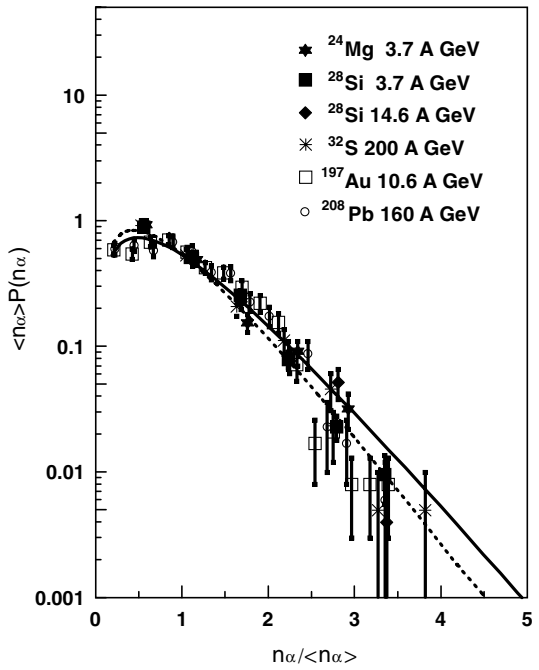

Fig. 5. $\langle n_\alpha \rangle P(n_\alpha)$ distribution as a function of the scaled variable $n_\alpha/\langle n_\alpha \rangle$ for helium fragments for different projectiles incident on emulsion target nuclei at different energies compared with the universal KNO scaling. Symbols are the experimental data while the solid and dashed curves are the results of eqs. (3) and (4), respectively (see text for details).

rather than to the others. From this one may conclude that the fragmentation of projectiles, which is responsible for the production of He-fragments, is evidently influenced by the impact parameter of the collision.

The multiplicity distributions of the produced fragments have been regarded as a potentially useful source of information of the underlying production mechanism. The multiplicity distributions of helium fragments (via the decay properties of the excited projectile) in relativistic nucleus-nucleus (AA) collisions using the two-source emission picture hade been analyzed by numerous authors [36–42]. Following ref. [39], the multiplicity distributions of the helium fragments produced in nuclear interactions with emulsion nuclei at different beam energies conveniently compared using the Koba-Nielsen-Olesen (KNO) scaling [20]. This scaling is a consequence of the nuclear geometry, which is energy independent. When, multiplicities of produced alpha particles, n_α, are studied in the scaling variables,

$$\Psi(Z) = 4Z \exp(-2Z) \tag{3a}$$

with

$$\Psi(Z) = \langle n_\alpha \rangle P(n_\alpha) = \langle n_\alpha \rangle \sigma_{n\alpha}/\sigma_{\rm nuc}, \tag{3b}$$

the data fall on the same universal curve. Where the scaled variable $Z = n_\alpha/\langle n_\alpha \rangle$ is the number of alpha-particles produced in an event normalized by the average helium multiplicity of the whole data sample, $P(n_\alpha)$ is the probability of finding n_α fragments in the final state, $\sigma_{n\alpha}$ denotes the partial cross-section for producing a state of multiplicity of n_α and $\sigma_{\rm nuc}$ is the total nuclear cross-section.

In refs. [36–42], it was shown that the multiplicity of the produced helium fragments from the events of different projectiles over a wide range of energies can be represented by a universal the experimental function of the following form:

$$\Psi(Z) = AZ \exp(-BZ), \tag{4}$$

where A and B are constants, whose values used in literature are different. We adopted a χ^2 minimization method to determine a unique value for each of A and B which best fits all experimental points.

Figure 5 presents the multiplicity distribution of $\langle n_\alpha \rangle P(n_\alpha)$ as a function of the scaled variable $n_\alpha/\langle n_\alpha \rangle$ for the helium fragments considered through all this work, which are then compared also to the universal KNO scaling. The different symbols are the experimental data, while the solid and dashed curves are the results of eqs. (3) and (4), respectively. The same kind of plot is shown in fig. 6 for the 3.7 A GeV ^{24}Mg projectile data as a function of H, CNO and AgBr emulsion nuclei. The data points corresponding to the different beams at different energies in fig. 5 as well as the different targets in fig. 6 fall on top of each other and fit with the universal curves. It is interesting to note that the multiplicity distributions of helium projectile fragments emerged in the interactions of different projectile nuclei with the different target emulsion nuclei at different energies are well described by the KNO scaling presentation. The best fit results from the dashed curves, which are the graphical presentation of eq. (4) with the parameters $A = 5.10 \pm 0.11$ and $B = 2.23 \pm 0.07$ for all projectile and target nuclei at all energies.

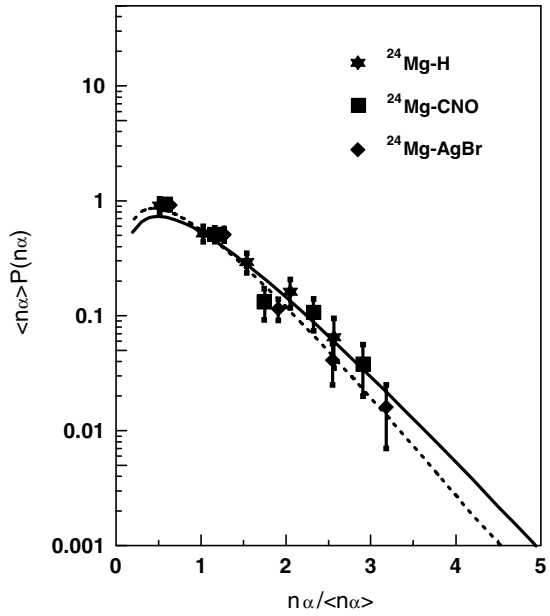

Fig. 6. $\langle n_\alpha \rangle P(n_\alpha)$ distribution as a function of the scaled variable $n_\alpha/\langle n_\alpha \rangle$ for helium fragments emitted in the 3.7 A GeV ^{24}Mg interactions with the different targets of emulsion compared with the universal KNO scaling. Symbols are the experimental data while the solid and dashed curves are the results of eqs. (3) and (4), respectively (see text for details).

If multiplicity scaling is valid, as a consequence also the moments defined in cite37,40,41 by

$$C_q = \langle n_\alpha^q \rangle / \langle n_\alpha \rangle^q \tag{5}$$

for q = 2, 3, 4 and 5 relative to the helium fragments, should be energy independent. To test the validity of KNO scaling, the multiplicity distributions using the C_q as given by eq. (5) should be studied. Table 2 presents the results on the average multiplicities and the moments C_2, C_3, C_4 and C_5 of the fast helium fragments emitted from the collision of 3.7 A GeV ^{24}Mg projectile with the target emulsion nuclei (H, CNO, Em, AgBr) compared with the corresponding values for ^{12}C, ^{16}O, ^{22}Ne, ^{28}Si, ^{32}S, ^{197}Au and ^{208}Pb beams at various energies. The second Muller moment [43] can be calculated from the following equation:

$$F_2 = (C_2 - 1)\langle n_\alpha \rangle^2 - \langle n_\alpha \rangle. \tag{6}$$

and it is included in table 2 for all projectiles and energies here considered. It is clear that the values of C_2 and C_3 moments, within the experimental errors, do not seem to depend upon the energy or masses the colliding nuclei. On the other hand, the higher moments C_3, C_4 and C_5 show a slow increase in their values as the projectile mass number increases. The second Muller moments are nonzero: this may indicate a strong correlation among the helium fragments. In addition to that, the mean multiplicity $\langle n_\alpha \rangle$ derived in the interactions of different projectiles at various incident energies can be satisfactory described in terms of the projectile mass number A_p by the following power law:

$$\langle n_\alpha \rangle = c A_\mathrm{p}^\mathrm{d} \tag{7}$$

where $c = 0.37 \pm 0.02$ and $d = 0.47 \pm 0.01$. An interesting observation of these experiments is that the value of the ratio $\langle n_\alpha \rangle / D$ $(D = \langle n_\alpha^2 \rangle - \langle n_\alpha \rangle^2)$ for all projectiles (see table 2) is approximately equal to constant revealing that asymptotic multiplicity scaling and is equal to that observed in hadron-nucleus interactions [37]. These exhibit an almost identical behavior in all beams at different energies, which leads to an energy and masses of colliding nuclei independent effect mechanism on the breakup of projectile nuclei through He fragments [36].

The mean multiplicities of the different charged secondary particles emitted from the interactions of 3.7 A GeV ^{24}Mg with the different components of emulsion nuclei at various ranges of projectile fragments (different degrees of disintegration of the projectile nucleus) are displayed in table 3. It is clear that as the number of He fragments not associated to any heavy fragments of charge $Z \geqslant 3$ increases (increasing peripherality), the values of $\langle n_\mathrm{s} \rangle$ decrease rapidly, while the values of $\langle n_\mathrm{g} \rangle$, $\langle n_\mathrm{b} \rangle$ and $\langle n_\mathrm{h} \rangle$ decrease slowly. The dependence of the average multiplicities of these secondaries on the target mass is also displayed in table 3 for the interactions of ^{24}Mg projectile with H, CNO and AgBr groups of target nuclei. One can see that the averages $\langle n_\mathrm{i} \rangle$ (i = s, g, b, h) increase substantially with increasing target mass. It is evident that the multiplicities of all types of charged particles depend strongly on the impact parameter of nucleus-nucleus collisions. On the other hand, the values of $\langle n_\mathrm{i} \rangle$ in the events in which the fast helium fragments are accompanied by heavy fragments having $Z \geqslant 3$ seem to be constant as the He-multiplicity increases, and exhibit a behavior independent of the He-multiplicity. These events can be considered coming from more peripheral collisions, indicating that the participant parts from both projectile and target nuclei are very small and the energy transferred from the projectile to the target is nearly constant. The present measurements are seen to be in systematic agreement with the values obtained from the 14.6 A GeV ^{28}Si interactions in nuclear emulsion [36]. The average numbers of slow target fragments $\langle n_\mathrm{b} \rangle$ emitted from the 3.7 A GeV ^{24}Mg and 14.6 A GeV ^{28}Si-induced emulsion reactions are the same, within experimental errors. The latter fact indicates that the fragments evaporated from the target do not seem to depend either on the energy or on the mass of the beam.

4 Conclusions

In the present paper we have studied the properties of the relativistic helium fragments emitted from the projectile in the interactions of ^{24}Mg ions accelerated at an energy of 3.7 A GeV with emulsion nuclei and the results obtained from this investigation allow us to make the following conclusions:

– The total and partial nuclear cross-sections of helium fragmentation channels in relativistic and ultrarelativistic nucleus-nucleus collisions are energy independent and for n_α = 1 and 2 they increase when the masses of both projectile and/or target increase.

Table 3. Dependence of the measured average values of secondary charged particles on the number of helium fragments without heavy fragments in the same event, associated with heavy fragments having charge $Z \geqslant 3$, and with all projectile fragments from the interactions of 3.7 A GeV ^{24}Mg projectile with the different groups of emulsion nuclei.

Reaction	multiplicities	1α	2α	3α	4α	All α's
Without projectile fragment having charge $Z \geqslant 3$						
^{24}Mg-H	$\langle n_s \rangle$	7.67 ± 0.76	5.89 ± 0.70	3.76 ± 0.57	3.09 ± 0.31	4.56 ± 0.39
	$\langle n_g \rangle$	0.33 ± 0.21	0.33 ± 0.17	0.47 ± 0.12	0.27 ± 0.14	0.30 ± 0.07
	$\langle n_b \rangle$	0.00	0.33 ± 0.17	0.06 ± 0.06	0.09 ± 0.09	0.12 ± 0.05
^{24}Mg-CNO	$\langle n_s \rangle$	11.90 ± 0.57	9.08 ± 0.68	6.86 ± 0.87	3.77 ± 0.71	9.13 ± 0.46
	$\langle n_g \rangle$	3.23 ± 0.24	2.92 ± 0.26	2.50 ± 0.47	2.15 ± 0.30	2.88 ± 0.15
	$\langle n_b \rangle$	1.85 ± 0.22	1.86 ± 0.24	1.79 ± 0.39	2.23 ± 0.46	1.89 ± 0.14
^{24}Mg-Em	$\langle n_s \rangle$	15.05 ± 0.63	10.79 ± 0.52	7.47 ± 0.69	3.86 ± 0.43	11.06 ± 0.39
	$\langle n_g \rangle$	9.31 ± 0.79	6.40 ± 0.50	3.68 ± 0.58	2.82 ± 0.71	6.61 ± 0.39
	$\langle n_b \rangle$	6.69 ± 0.54	5.95 ± 0.54	3.45 ± 0.75	3.07 ± 0.89	5.47 ± 0.32
^{24}Mg-AgBr	$\langle n_s \rangle$	16.90 ± 0.84	11.94 ± 0.67	9.60 ± 0.89	8.02 ± 0.93	13.93 ± 0.55
	$\langle n_g \rangle$	13.14 ± 0.95	9.74 ± 0.56	8.20 ± 0.74	8.66 ± 0.83	11.16 ± 0.54
	$\langle n_b \rangle$	9.91 ± 0.57	9.48 ± 0.59	8.40 ± 0.95	10.18 ± 0.90	9.63 ± 0.38
With projectile fragment having charge $Z \geqslant 3$						
^{24}Mg-H	$\langle n_s \rangle$	2.18 ± 0.24	1.96 ± 0.40			2.13 ± 0.21
	$\langle n_g \rangle$	0.30 ± 0.07	0.17 ± 0.08			0.28 ± 0.05
	$\langle n_b \rangle$	0.12 ± 0.05	0.21 ± 0.08			0.15 ± 0.04
^{24}Mg-CNO	$\langle n_s \rangle$	4.42 ± 0.43	3.67 ± 0.87			4.18 ± 0.39
	$\langle n_g \rangle$	2.30 ± 0.16	2.11 ± 0.43			2.24 ± 0.15
	$\langle n_b \rangle$	2.29 ± 0.19	1.89 ± 0.34			2.20 ± 0.17
^{24}Mg-Em	$\langle n_s \rangle$	4.65 ± 0.29	3.64 ± 0.48	2.25 ± 0.82	2.02 ± 0.52	4.34 ± 0.25
	$\langle n_g \rangle$	3.18 ± 0.28	2.58 ± 0.56	1.38 ± 0.71	0.34 ± 0.21	2.99 ± 0.25
	$\langle n_b \rangle$	3.11 ± 0.27	2.21 ± 0.48	1.13 ± 0.52	0.83 ± 0.48	2.84 ± 0.23
^{24}Mg-AgBr	$\langle n_s \rangle$	7.05 ± 0.63	6.11 ± 0.84			6.82 ± 0.53
	$\langle n_g \rangle$	7.90 ± 0.65	8.00 ± 0.96			7.88 ± 0.61
	$\langle n_b \rangle$	7.91 ± 0.55	7.01 ± 0.83			7.66 ± 0.52
With all projectile fragments						
^{24}Mg-H	$\langle n_s \rangle$	2.77 ± 0.34	3.03 ± 0.46	3.76 ± 0.57	3.09 ± 0.31	2.99 ± 0.22
	$\langle n_g \rangle$	0.30 ± 0.06	0.21 ± 0.07	0.47 ± 0.12	0.27 ± 0.14	0.29 ± 0.04
	$\langle n_b \rangle$	0.11 ± 0.04	0.24 ± 0.05	0.06 ± 0.06	0.09 ± 0.09	0.14 ± 0.03
	$\langle n_h \rangle$	0.41 ± 0.07	0.45 ± 0.09	0.53 ± 0.12	0.36 ± 0.15	0.43 ± 0.05
^{24}Mg-CNO	$\langle n_s \rangle$	7.17 ± 0.49	7.31 ± 0.66	6.86 ± 0.87	3.77 ± 0.71	6.87 ± 0.35
	$\langle n_g \rangle$	2.64 ± 0.14	2.65 ± 0.23	2.50 ± 0.47	2.15 ± 0.30	2.58 ± 0.11
	$\langle n_b \rangle$	2.13 ± 0.15	1.86 ± 0.19	1.79 ± 0.39	2.23 ± 0.46	2.03 ± 0.11
	$\langle n_h \rangle$	4.77 ± 0.17	4.53 ± 0.24	4.29 ± 0.53	4.38 ± 0.59	4.63 ± 0.13
^{24}Mg-Em	$\langle n_s \rangle$	8.60 ± 0.42	8.25 ± 0.47	6.57 ± 0.65	3.86 ± 0.43	7.98 ± 0.28
	$\langle n_g \rangle$	5.51 ± 0.39	5.04 ± 0.41	3.28 ± 0.51	2.82 ± 0.71	4.95 ± 0.25
	$\langle n_b \rangle$	4.47 ± 0.28	4.62 ± 0.41	3.04 ± 0.64	3.07 ± 0.89	4.26 ± 0.21
	$\langle n_h \rangle$	9.98 ± 0.63	9.66 ± 0.78	6.33 ± 1.07	5.89 ± 0.98	9.26 ± 0.44
^{24}Mg-AgBr	$\langle n_s \rangle$	13.28 ± 0.74	11.11 ± 0.64	9.60 ± 0.89	8.02 ± 0.93	12.10 ± 0.49
	$\langle n_g \rangle$	11.22 ± 0.69	9.49 ± 0.55	8.20 ± 0.74	8.66 ± 0.83	10.31 ± 0.44
	$\langle n_b \rangle$	9.17 ± 0.42	9.13 ± 0.56	8.40 ± 0.95	10.18 ± 0.90	9.12 ± 0.32
	$\langle n_h \rangle$	20.39 ± 0.97	18.62 ± 0.96	16.60 ± 1.19	18.84 ± 1.25	19.44 ± 0.65

– The production rate of one helium fragment is about two times that of two helium and four times $n_\alpha = 3$ in the case of ^{24}Mg, ^{28}Si and ^{32}S projectiles.
– The stripping rates of the fast-moving helium fragments in ^{197}Au and ^{208}Pb beams are much broader and extended up to 16α.
– There are no significant difference, within the statistical errors, in the yields of He fragments emitted in the interactions of ^{24}Mg with H, light CNO and heavy AgBr groups of emulsion nuclei, indicating that the emission of fast-moving helium fragments from the projectile is also target independent.
– The validity of the assumption of the limiting fragmentation behavior of fast-moving helium fragments is fulfilled in the energy range 3–200 A GeV for both the projectile and target nuclei.

- We may point out that the nuclear fragments produced in high-energy heavy-ion collisions have two emission sources: the contact layer and the other part of the spectator [39]. Based on the two-source emission picture, a kind of KNO scaling is obtained and describes the multiplicity distribution of fast-moving helium projectile fragments. It is interesting to note that the multiplicity distributions of helium projectile fragments emitted in the interactions of different projectile with different target emulsion nuclei at different energies are well described by the KNO scaling presentation.
- As the C_q moments should be energy independent in order to validate the KNO scaling, the values of the moments have been checked. The values of C_2 and C_3 moments, within the experimental errors, do not seem to depend upon the energy or masses the colliding nuclei. On the other hand, the higher moments C_3, C_4 and C_5 show a slow increase in their values as the projectile mass number increases. The second Muller moments are nonzero, indicating that a strong correlation among the helium fragments exists.
- The mean multiplicities of the different charged secondary particles $\langle n_{\rm s}\rangle$, $\langle n_{\rm g}\rangle$ and $\langle n_{\rm b}\rangle$ emitted from the interactions of 3.7 A GeV ^{24}Mg with emulsion nuclei at different ranges of projectile fragments (different degrees of disintegration of the projectile nucleus) are decreasing as far as the number of He fragments not associated with any heavy fragments of charge $Z \geqslant 3$ increases (increasing peripherality).
- The averages $\langle n_{\rm i}\rangle$ (i = s, g, b, h) increase substantially with increasing target mass from H up to AgBr underlying that the multiplicities of all types of charged particles depend strongly on the impact parameter of nucleus-nucleus collisions. The values of $\langle n_{\rm i}\rangle$ in those events in which the fast helium fragments have been accompanied by heavy fragments with $Z \geqslant 3$ seem to be constant as the He-multiplicity increases, and exhibit a behavior independent of the He-multiplicity. These events are related to more peripheral collisions, where the participant parts of the projectile and target are supposed to be very small and the energy transfer between the two colliding nuclei is almost constant.
- The average numbers of slow target fragments $\langle n_{\rm b}\rangle$ emitted from interactions of the 3.7 A GeV ^{24}Mg (present work) and 14.6 A GeV ^{28}Si [36] on the emulsion targets are, within experimental errors, the same. This fact indicates that the target evaporation fragments do not seem to depend either on the energy or on the mass of the beam.

References

1. P.L. Jain, G. Singh, A. Mukhopadhyay, Phys. Rev. C **50**, 1085 (1994).
2. G. Singh, P.L. Jain, Phys. Rev. C **54**, 3185 (1996) and references therein.
3. M.A. Jilany, Phys. Rev. C **70**, 014901 (2004).
4. K.A. Chikin, V.L. Korotkih, A.P. Kryukov, L.I. Sarycheva, I.A. Pshenichnov, J.P. Bondorf, I.N. Mishustin, Eur. Phys. J. A **8**, 537 (2000).
5. J. Hüfner, Phys. Rep. **125**, 129 (1985).
6. D.H.E. Gross, Rep. Prog. Phys. **53**, 605 (1990) and references therein.
7. J. Bondorf *et al.*, Phys. Rep. **257**, 133 (1995); J. Bondorf *et al.*, Nucl. Phys. A **444**, 460 (1985).
8. M.I. Adamovich *et al.*, Eur. Phys. J. A **5**, 429 (1999) and references therein.
9. Y.D. Kim *et al.*, Phys. Rev. Lett. **63**, 494 (1989).
10. C.A. Ogivie *et al.*, Phys. Rev. Lett. **67**, 1214 (1991).
11. M.L. Cherry *et al.*, Eur. Phys. J. C **5**, 641 (1998).
12. M.L. Cherry *et al.*, Phys. Rev. C **52**, 2652 (1995).
13. D.G. d'Enterria *et al.*, Phys. Rev. C **52**, 3179 (1995).
14. W. Trautmann, Preprint nucl-ex/9611002.
15. J. Lee, A.Z. Mekjian, Nucl. Phys. A **730**, 514 (2004) and references therein.
16. G.F. Bertsch, S. Das Gupta, Phys. Rep. **160**, 189 (1988).
17. G. Peilert *et al.*, Phys. Rev. C **39**, 1402 (1989); J. Aichelin, Phys. Rep. **202**, 233 (1991).
18. A. Aranda, C.O. Dorso, V. Furci, J.A. Lopez, Phys. Rev. Lett. **52**, 3217 (1995).
19. M.I. Adamovich *et al.*, Nucl. Phys. A **593**, 535 (1995) and references therein.
20. Z. Koba, H.B. Nielsen, P. Olesen, Nucl. Phys. B **40**, 317 (1972).
21. H.E. Stanley, *Introduction to Phase Transitions and Critical Phenomena* (Clarendon Press, 1971).
22. M.A. Jilany, Nucl. Phys. A **705**, 477 (2002) and references therein.
23. B.K. Singh, S.K. Tuli, Nuovo Cimento A **112**, 1093 (1999).
24. M. El-Nadi, M.S. El-Nagdy, N. Ali-Mossa, A. Abdelsalam, A.M. Abdalla, A.A. Hamed, J. Phys. G **25**, 1169 (1999).
25. H.L. Bradt, B. Peters, Phys. Rev. **77**, 54 (1950).
26. M. El-Nadi, A. Abdelsalam, M.S. El-Nagdy, E.A. shaat, N. Ali-Mossa, Z. Abou-Moussa, S. Kamel, N. Rashed, M.E. Hafiz, B. Badawy, *Proceedings of the 27th International Cosmic Ray Conference, Hamburg, Germany, 7-15 August 2001* (Copernicus Gesellschaft, Katlenburg-Lindau, 2001) p. 1366.
27. M. El-Nadi, A. Abdelsalam, N. Ali-Mossa, Z. Abou-Moussa, Kh. Abdel-Waged, W. Osman, B. Badawy, Nuovo Cimento A **111**, 1243 (1998).
28. M. Nabil. Yasin, M.M. Sherif, S.M. Abd El-Halim, M.A. Jilany, Sov. Phys JETP **84**, 635 (1997).
29. M.I. Adamovich *et al.*, Sov. J. Nucl. Phys. **29**, 52 (1979).
30. M.I. Adamovich *et al.*, Phys. Rev. Lett. **62**, 2801 (1989).
31. Alma-Ata-Bucharest-Gatchina-Dubna-Dushanbe-Erevan-Kosice-Krakow-Leningrad-Moscow-Rzezz-Tashkent-Tbilisi-Ulaan-Bator Collaboration, Sov. J. Nucl. Phys. **45**, 78 (1987).
32. M.I. Adamovich *et al.*, Z. Phys. A **351**, 311 (1995); B.K. Singh, I.D. Ojha, S.K. Tuli, Nucl. Phys. A **570**, 819 (1994).
33. S.Y.Bahk *et al.*, Phys. Rev. C **43**, 1410 (1991).
34. A. Abdelsalam, E.A. Shaat, N. Ali-Mossa, Z. Abou-Moussa, O.M. Osman, N. Rashed, W. Osman, B.M. Badawy, E. El-Falaky, J. Phys. G **28**, 1375 (2002).
35. G. Baroni *et al.*, Nucl. Phys. A **516**, 673 (1990).
36. M. El-Nadi, M.S. El-Nagdy, N. Ali-Mossa, A. Abdelsalam, A.M. Abdalla, S.M. Abdel-Halim, J. Phys. G **28**, 1251 (2002).
37. G. Singh, A.Z.M. Ismail, P.L. Jain, Phys. Rev. C **43** , 2417 (1991); G. Singh, K. Sengupta, P.L. Jain, Phys. Rev. C **42**, 1757 (1990); Phys. Lett. B **222**, 301 (1989).
38. S. Kamel, Nuovo Cimento A **112**, 733 (1999).

39. Fu-Hu Liu, Y.A. Panebratsev, Nuovo Cimento A **111**, 1219 (1998); Fu-Hu Liu, Phys. Rev. C **62**, 024613 (2000).
40. M. El-Nadi, M.M. Sherif, A. Abd El-salam, M.N. Yasin, A. Bakr, M.S. El-Nagdy, M.A. Jilany, Int. J. Mod. Phys. E **2**, 381 (1993).
41. P.L. Jain, M.M. Aggarwal, Phys. Rev. C **33**, 1970 (1986).
42. L.S. Liu, T.C. Meng, Phys. Rev. D **27**, 2640 (1983).
43. A.H. Muller, Phys. Rev. D **4**, 150 (1971).